Quaternary Science Reviews 138 (2016) 49–61

Contents lists available at ScienceDirect

Quaternary Science Reviews

journal homepage: www.elsevier.com/locate/quascirev

Tracking millennial-scale Holocene glacial advance and retreat using osmium isotopes: Insights from the Greenland ice sheet

Alan D. Rooney [a, b, *], David Selby [b], Jeremy M. Lloyd [c], David H. Roberts [c], Andreas Lückge [d], Bradley B. Sageman [e], Nancy G. Prouty [f]

[a] Department of Earth and Planetary Sciences, Harvard University, Cambridge, MA, 02138, USA
[b] Department of Earth Sciences, Durham University, Durham, DH1 3LE, UK
[c] Department of Geography, Durham University, Durham, DH1 3LE, UK
[d] Bundesanstalt für Geowissenschaften und Rohstoffe, Stilleweg 2, 30655, Hannover, Germany
[e] Department of Earth and Planetary Sciences, Northwestern University, 1850 Campus Drive, Evanston, IL, USA
[f] US Geological Survey, Pacific Coastal & Marine Science Center, 400 Natural Bridges Drive, Santa Cruz, CA 95060, USA

ARTICLE INFO

Article history:
Received 3 August 2015
Received in revised form
15 February 2016
Accepted 19 February 2016
Available online xxx

Keywords:
Greenland ice sheet
Osmium
Holocene
Ocean-ice interaction

ABSTRACT

High-resolution Os isotope stratigraphy can aid in reconstructing Pleistocene ice sheet fluctuation and elucidating the role of local and regional weathering fluxes on the marine Os residence time. This paper presents new Os isotope data from ocean cores adjacent to the West Greenland ice sheet that have excellent chronological controls. Cores MSM-520 and DA00-06 represent distal to proximal sites adjacent to two West Greenland ice streams. Core MSM-520 has a steadily decreasing Os signal over the last 10 kyr ($^{187}Os/^{188}Os$ = 1.35–0.81). In contrast, Os isotopes from core DA00-06 (proximal to the calving front of Jakobshavn Isbræ) highlight four stages of ice stream retreat and advance over the past 10 kyr ($^{187}Os/^{188}Os$ = 2.31; 1.68; 2.09; 1.47). Our high-resolution chemostratigraphic records provide vital benchmarks for ice-sheet modelers as we attempt to better constrain the future response of major ice sheets to climate change. Variations in Os isotope composition from sediment and macro-algae (seaweed) sourced from regional and global settings serve to emphasize the overwhelming effect weathering sources have on seawater Os isotope composition. Further, these findings demonstrate that the residence time of Os is shorter than previous estimates of ~10^4 yr.

1. Introduction

The Greenland Ice Sheet (GrIS) is the largest ice reservoir in the Arctic containing the equivalent of *c.* 7 m of global sea level and numerical modeling suggests the GrIS could contribute >0.5 m of global sea level rise by A.D. 2100 (Gregory et al., 2004; Pfeffer et al., 2008). The large volumes of icebergs and meltwater delivered from the GrIS can produce major changes in ocean circulation, ecosystems and, ultimately, affect climate (McManus et al., 2004; Christoffersen and Hambrey, 2006; Raiswell et al., 2006). Direct observations of the GrIS have revealed rapid changes in mass balance on sub-decadal time scales in response to changing climate forcing (Joughin et al., 2004; Rignot and Kanagaratnam, 2006; Howat et al., 2007; Holland et al., 2008; Nick et al., 2009; Straneo et al., 2013; Khan et al., 2015). However, the drivers and mechanisms of longer-term, climatic changes to polar ice sheets are less well understood.

At the end of the Last Glacial Maximum (LGM) the GrIS extended onto the continental shelf of Greenland (Roberts et al., 2010; Funder et al., 2011; Ó Cofaigh et al., 2013). Evidence from periglacial features, sedimentary archives, fossil foraminifera assemblages and $\delta^{18}O$ records from benthic foraminifera suggest that the ice margin in West Greenland underwent numerous, extensive advances and retreats due to fluctuations in atmospheric and ocean temperatures during the LGM/Holocene transition and within the Holocene (Long et al., 2006; Young et al., 2011, 2013; Lane et al., 2014). In this paper we explore the duration and amplitude of these ice sheet fluctuations using nearshore sedimentary sequences where coupled sedimentological and geochemical studies can potentially elucidate ice sheet response to centennial and millennial-scale climatic forcings. In particular, we present osmium isotopic data from three

* Corresponding author. Department of Earth and Planetary Sciences, Harvard University, Cambridge, MA, 02138, USA.
E-mail address: alanrooney@fas.harvard.edu (A.D. Rooney).

http://dx.doi.org/10.1016/j.quascirev.2016.02.021

sediment cores from the western Greenland margin that document rapid responses of the ice sheet to changing climate through the Holocene.

Radiogenic isotopes have previously been employed to assess large-scale variations in continental weathering rates related to glacial-interglacial cycles (e.g. Farmer et al., 2003; Colville et al., 2011). The Sr-Nd-Pb isotope systems have been used to evaluate changes in seawater chemistry during Pleistocene glacial-interglacial periods and shown to respond to fluctuations in ice sheet mass (Blum and Erel, 1995; Farmer et al., 2003; Colville et al., 2011; Flowerdew et al., 2013; Jonkers et al., 2015). Osmium (Os) isotopes ($^{187}Os/^{188}Os$) have also been used to understand the interplay between silicate weathering, and palaeoceanographic processes during the Pleistocene glacial-interglacial cycles, Late Ordovician and Neoproterozoic glacial events (Oxburgh, 1998; Peucker-Ehrenbrink and Ravizza, 2000; Williams and Turekian, 2004; Dalai et al., 2005; Dalai and Ravizza, 2006; Oxburgh et al., 2007; Paquay et al., 2009; Burton et al., 2010; Finlay et al., 2010; Paquay and Ravizza, 2012; Rooney et al., 2014).

For the Pleistocene glacial-interglacial cycles Os isotope data from global sites display heterogeneous profiles, which are interpreted to reflect changes in the local Os seawater composition of individual basins resulting from greater oceanographic restriction rather than changes in silicate weathering rates across the glacial-interglacial periods (Paquay and Ravizza, 2012). A similar oceanographic control on seawater $^{187}Os/^{188}Os$ compositions is observed for global sites during the ice-free Cretaceous world (*c.* 94 Ma, Du Vivier et al., 2014, 2015).

To help understand the complexities of palaeoceanography that potentially control the Os data shown for the Pleistocene glacial-interglacial cycles we investigate the use of Os isotopes to track Holocene variability of the GrIS in the Disko Bugt-Uummannaq region. This study focuses on three time-correlated sedimentary sequences: one proximal to the GrIS currently influenced by seasonal meltwater flux; one intermediate site mid-way across the continental shelf; and one in a distal setting beyond the continental shelf on the northern edge of the Labrador Sea (Fig. 1). All sites have been previously studied for their biostratigraphy, sedimentology and chronology (Lloyd et al., 2005; McCarthy, 2011; Knutz et al., 2011), and are adjacent to ice sheet catchments with well-constrained glacial histories. At the LGM the GrIS extended 300–400 km across the continental shelf in the Uummannaq – Disko Bugt region and was grounded at the shelf edge (Ó Cofaigh et al., 2013; Jennings et al., 2014). A combination of radiocarbon dating and cosmogenic radiogenic nuclide dating has been used to track ice retreat through the Uummannaq and Disko fjord systems (Lloyd et al., 2005; Young et al., 2013; Ó Cofaigh et al., 2013; Roberts et al., 2013; Lane et al., 2014). By integrating the new Os isotope data with current palaeoceanographic model(s) we demonstrate the ability of Os to reconstruct ice sheet fluctuations, and that oceanographic setting critically controls the $^{187}Os/^{188}Os$ composition of the seawater.

2. Studied sites and sample material

The three study sites are located along a transect from proximal to distal in relation to the present day GrIS as follows: Core DA00-06 from a proximal setting <10 km from the mouth of Jakobshavn Isfjord within Disko Bugt; Core MSM-520 from an intermediary location *c.* 70 km northwest of the Nuussuaq Peninsula mid-way across the shelf within the Uummannaq fjord and; Core DA-04-31T from a distal location beyond the continental shelf *c.* 200 km southwest of Nuuk at the northern edge of the Labrador Sea (Fig. 1A, B). Hypothetically these three cores should record changing Os isotopes in different environments relative to the ice margin as all three regions are at the convergence of multiple water masses (Fig. 1) and are sourcing Os from highly variable bedrock lithologies (Table 1; Fig. 2). In addition, we have sampled bedrock, other surface sediments, and algae for comparison to nearby source regions and far field areas not affected by the GrIS.

2.1. Core DA00-06

This is a 960 cm long piston core collected from a water depth of 363 m by the *R/V Dana* in 2000 (Table 2). This core spans *c.* 9.0 ka based on six Accelerator Mass Spectrometry (AMS) radiocarbon dates and records deposition proximal to the mouth of the Jakobshavn Isbræ in Disko Bugt (Lloyd et al., 2005; Hogan et al., 2011, Table 2). Sediments comprise blue-grey silty organic matter-bearing clay with occasional ice rafted clasts from the base of the core up to 100 cm where there is a transition to a clast dominated organic matter-bearing sandy silt to the top of the core (Lloyd et al., 2005). The lithology and biostratigraphy are interpreted to document the retreat of Jakobshavn Isbræ across inner Disko Bugt and into Jakobshavn Isfjord. High sedimentation rates in the lower section of the core (13.8 mm a^{-1}) and a predominance of glaciomarine benthic foramininferal fauna are suggestive of a still-stand in retreat as the ice stream was pinned on the sill of Jakobshavn Isfjord from 9.0 to 7.6 ka cal. BP (Fig. 3A; Lloyd et al., 2005). After *c.* 7.6 ka the ice stream retreated into the main fjord system and sedimentation rates fell to 0.24 mm a^{-1} for the upper 100 cm of the core with an Atlantic water influenced benthic foraminiferal assemblage dominating (Fig. 3A). This switch in fauna is indicative of increasing influence of the relatively warm and saline West Greenland Current at the core site from *c.* 7.6 ka (Lloyd et al., 2005). A radiocarbon date of 9.0 ka cal. BP from near the base of the core provides a minimum age constraint for deglaciation in this region of Disko Bugt (Lloyd et al., 2005).

2.2. Core MSM-520

This 1200 cm gravity core was recovered from a water depth of 545 m during a cruise of the *R/V Maria S Merian* in 2007. The core records sedimentation over the last *c.* 11 ka based on 10 AMS radiocarbon dates (McCarthy, 2011; Tables 2 and 3). The sediments from the lower section of the core (from 990 to 879 cm) are composed of rigid, blue-grey, silty organic matter-bearing clay with abundant coarse clasts. From 879 cm there is a transition to softer more clay rich sediments with scattered ice rafted clasts through the rest of the core (McCarthy, 2011). Based on the sedimentology and benthic foraminiferal assemblage the lower section of the core from 990 to 879 cm has been interpreted as a subglacial till (very stiff diamicton with no foraminifera). Towards the top of this unit and at the transition to the overlying sediments benthic foraminifera are initially dominated by typical glaciomarine species (e.g., *Elphidium excavatum f. clavata, Cassidulina reniforme*). The sedimentological and biostratigraphy data delineate the broad timing of the retreat of the ice stream through Uummannaq fjord with the core site being deglaciated by a minimum of 10.8 ka cal. BP (McCarthy, 2011). The benthic foraminiferal fauna record a gradual transition to a more distal glaciomarine environment by 8 ka cal. BP with the appearance of Atlantic water influenced species (e.g. *Adercotryma glomerata, Saccammina difflugiformis*) (McCarthy, 2011), indicating the increasing influence of the West Greenland Current at the core site (Fig. 3B). The biostratigraphy coupled with cosmogenic exposure ages from the Uummannaq Fjord region suggest that the ice streams had retreated to the near present-day location by *c.* 11–10 ka (Roberts et al., 2013; Lane et al., 2014). In summary, the sediments of core MSM-520 represent a more distal setting to the modern ice front in comparison to core DA00-06.

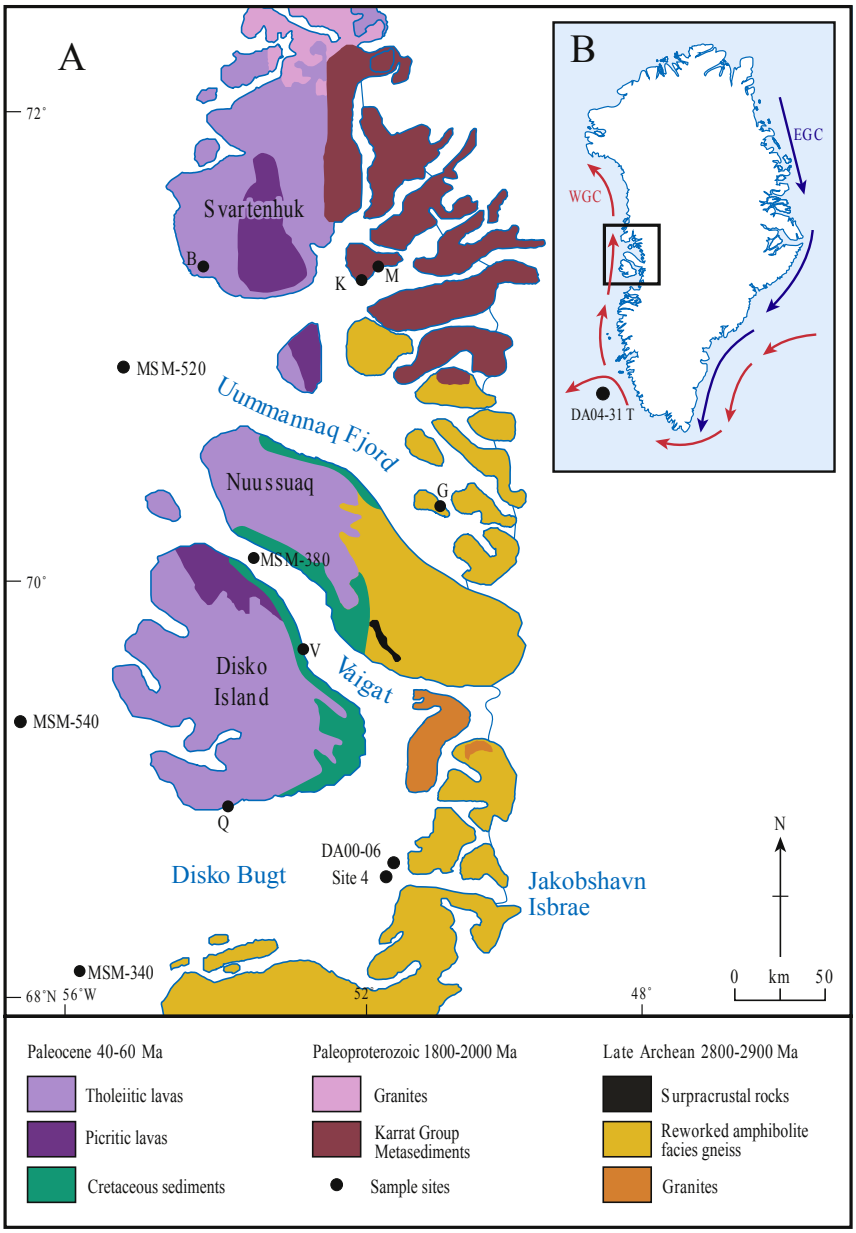

Fig. 1. Location maps. (A) Map showing location of Greenland related sediment, algae and bedrock sample sites mentioned in the text. Onshore geology of this region modified from Garde and Steenfelt (1999a,b). Abbreviations used: M–metagreywacke; B–basalt, G–Gneiss; Q–Qeqertarsuaq algae; K–Karratfjord algae; V–Vaigat algae. (B) Map showing ocean currents of Greenland and the study area of Disko Bugt (box in black outline). The inset map shows the location of Disko Bugt (box in black outline) and core DA04-31T. Abbreviations used; EGC–East Greenland Current (blue); WGC–West Greenland Current (red). (For interpretation of the references to colour in this figure legend, the reader is referred to the web version of this article.)

2.3. Core DA-04-31T

This core is a 78 cm long trigger core collected from a water depth of 2525 m during a cruise of the *R/V Dana* in 2004, adjacent to a longer piston core (878 cm long). The chronology of the main piston core was based on 12 AMS radiocarbon dates (Knutz et al., 2011). Lithostratigraphic correlations between the trigger core and piston core indicate that the trigger core (78 cm) records

Table 1
Sampling details for all cores and samples.

Sample and depth	Core length (cm)	Water depth (m)	Sedimentation rates (mm/yr)	Re range (ng/g)	Os range (pg/g)	Foraminifera species
DA04-31T	72	2525	0.02–0.16[a]	1.3–12	37–70	N-D
DA00-06	960	363	13–0.24	0.4–26	42–103	N-D
MSM-520	1200	545.7[b]	0.9	4–18	86–213	Lower sections: *Elphidium excavatum f. clavata* Upper sections:*Trochammina nana*

[a] Knutz et al. (2011).
[b] McCarthy (2011).

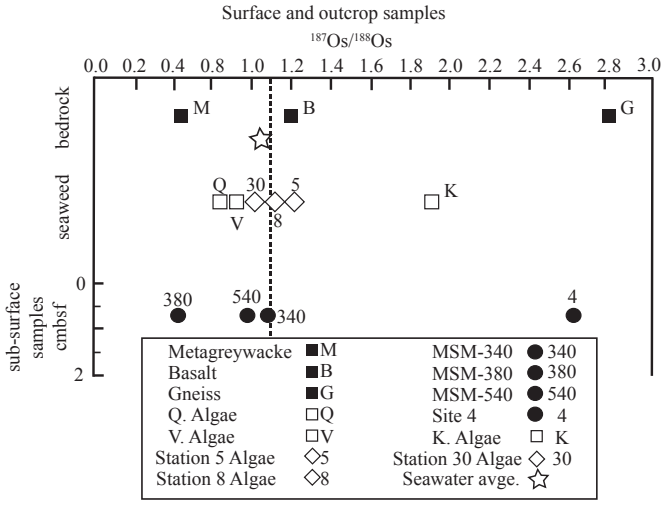

Fig. 2. Compilation of Os isotope ($^{187}Os/^{188}Os$) values of lithological samples (abbreviations are as in Fig. 1A), algae samples (additional abbreviations are; 5, 8 and 30–Station 5, 8 and 30, respectively) and shallow (2–4 cm below seafloor) sediment samples. Algae samples are taken from within the water column. Uncertainties on Os isotopes are 2σ and are smaller than all data points. See text for full details of algae locations and discussion.

sedimentation over the past *c.* 11 ka. Whilst this is not as accurate as the age models for the other cores it does provide strong support for the interpretation that DA-04-31T records sedimentation over the Holocene epoch. The sediments of the trigger core are composed of brown to grey silty organic matter-bearing clay with rare ice rafted clasts. The trigger core represents sedimentation in an open ocean setting, significantly beyond the continental shelf and direct influence from grounded ice. Knutz et al. (2011) identify a decreasing influence of meltwater from the retreating GrIS from *c.* 11–9 ka. From *c.* 9 ka the core site is more strongly influenced by a branch of the West Greenland Current that flows westward across the Davis Strait along the northern edge of the Labrador Sea (Knutz et al., 2011).

2.4. Surface sediments and algae from near Greenland

Four surface sediment samples from ≤5 cm below the seafloor were selected from locations in the Disko Bugt – Uummannaq area to characterize the modern-day seawater Os composition (MSM-340; 380; 540 and Site 4; Fig. 1B). All surface sediment samples were composed of brown to grey silty organic matter-bearing clay with occasional ice rafted clasts. Three brown macro-algae (seaweed) were obtained for Os isotope analysis from the coastal regions of Qeqertarsuaq (*Ascopyllum nodosum*), Vaigat (*Laminaria digitata*) and Karrat (*Fucus distichus*) fjords to complement the surface sediment samples (Fig. 1A).

2.5. Surface sediments and algae from far-field sites

To provide insight into the Os composition of the Holocene ocean for sediments deposited in non-glacial settings we also present data from the Laccadive Sea (core SO93, water depth of 1688 m, 140 miles southwest of Sri Lanka and India), Mentawai Strait (core SO189, water depth of 571 m, 20 miles off the coast of West Sumatra), and the Pacific Ocean (core SO161, water depth of 1001 m, 45 miles off the coast of Chile; Table 1). Lastly, we include data for three *Sargassum* seaweed samples collected from surface waters between 26 and 28°N and 87 and 89°W in the Gulf of Mexico (Table 1).

2.6. Greenland bedrock

Samples representative of the most common bedrock lithologies in the Disko Bugt – Uummannaq region were analyzed for their Re and Os elemental abundances and isotopic compositions in order to trace the sources of Os that determine the isotopic signal of seawater at the core sites (Fig. 1A). These lithologies are as follows; Archean tonalitic orthogneiss sampled from the island of Salliarususeq Storøen (70°40′05″N, 51°33′08″W), and Paleoproterozoic metagreywacke from the Nûkavsak Formation (71°31′18″N, 52°57′32″W) of the Karrat Group. A sample of basalt was taken from the Vaigat Formation on the Svartenhuk peninsula (71°31′10″N, 55°17′29″W).

3. Methods

3.1. TOC and Re–Os analytical protocols

Bedrock samples were cut and polished to remove any saw markings and together with soft sediment from sampled cores, dried at 60 °C for 48 h. Seaweed samples were rinsed with milliQ and dried at 60 °C for 24 h. Approximately 30–50 g for each rock or sediment sample was powdered in a Zirconia ceramic dish using a shatterbox to a fine (~30 μm) powder. For seaweed, a frond was ground in agate to a fine powder (~100 μm).

Powdered core samples were analyzed for weight percent concentration of total carbon (TC) by combustion at 950 °C in a stream of O_2, and total inorganic carbon (TIC) by acidification with 10% phosphoric acid. Sample carbon converted to CO_2 by each preparation method is quantified by coulometric titration (Huffman, 1977; Engleman et al., 1985). Analysis of standards and replicates indicates average uncertainty less than ±1%. Total organic carbon (TOC) is calculated as the difference between wt% TC and TIC. The TIC value is converted to wt% calcium carbonate by stoichiometric calculation (wt% TIC × 8.333), which assumes negligible quantities of inorganic carbon present as minerals other than calcium carbonate.

Rhenium and osmium abundances and isotope compositions were determined using isotope dilution negative thermal ionization mass spectrometry at the Durham University Laboratory for Source Rock and Sulfide Geochronology and Geochemistry using carius-tube digestion with solvent extraction, micro-distillation, and anion chromatography methods (Selby and Creaser, 2003; Cumming et al., 2013; Prouty et al., 2014).

In addition to being siderophilic and chalcophilic, Re and Os are organophilic. Rhenium and osmium in the water column are complexed to organic matter and with burial become preserved in organic-rich sediments (Ravizza and Turekian, 1989). In organic matter the Re and Os are predominantly bound to the kerogen fraction (Rooney et al., 2012). This study utilized the $Cr^{VI}O_3$– 4 N H_2SO_4 digestion technique, which has been shown to significantly limit the contribution of detrital Re and Os even in low TOC, and Re and Os bearing organic-rich rocks (e.g., Selby and Creaser, 2003; Kendall et al., 2004; Rooney et al., 2011; Kendall et al., 2013). Accurate and precise depositional Re–Os age determinations and Os isotope compositions of the water column contemporaneous with sediment deposition have been obtained from sedimentary rocks with as little as 0.5 wt% TOC, but also as low as 0.1 wt% TOC (Rooney et al., 2011, 2014; Harris et al., 2013; Selby et al., 2007; Kendall et al., 2013; Du Vivier et al., 2014, 2015; Rooney et al., 2014; Sperling et al., 2014). Average TOC values of the sample sets of this study are as follows: 0.27 wt% for core DA00-06; 1.25 wt% for core MSM-520; and 0.22 wt% for core DA-04-31T (Table 4). These values are higher than the average of 0.1 wt% reported by Sperling et al. (2014) suggesting that the Re–Os data presented here (generated using

Table 2
Re and Os elemental and isotopic composition data, calibrated ages and samples locations for surface samples and seaweed.

	w.t% TOC	% $CaCO_3$	Re (ng/g)	±	Os (pg/g)	±	^{192}Os (pg/g)	±	^{192}Os %	^{187}Re/^{188}Os	±	^{187}Os/^{188}Os	±	rho[a]	Osi[b]	±	Age cal. Kyr	Lat and long	Water depth (m)
Surface spot samples																			
MSM-340	1.77	1.24	6.37	0.021	118.2	0.8	43.2	0.2	36.5	293.7	2.7	1.13	0.01	0.65	1.13	0.01	0.01	68°36′55″N, 55°19′59″W	ND
MSM-380	ND	ND	1.65	0.005	126.7	0.6	50.0	0.2	39.5	65.6	0.6	0.48	0.01	0.65	0.48	0.01	0	70°19′04″N, 53°41′09″W	ND
MSM 380 r	ND	ND	1.57	0.01	117.7	2	46.4	0.9	37.2	67.3	2.7	0.50	0.03	0.70	0.50	0.02	–	–	ND
MSM-540	ND	ND	1.36	0.004	353.5	2.2	131.4	0.5	39.4	20.5	0.2	0.98	0.01	0.65	0.98	0.01	0	69°38′06″N, 57°26′03″W	ND
Site 4	0.14	0.59	1.94	0.019	36.5	0.4	11.4	0.1	31.2	339.3	6.7	2.62	0.05	0.76	2.62	0.04	0	69°08′00″N, 51°24′05″W	ND
Seaweed (Greenland)																			
Qeqertarsuaq (*Ascophyllum nodosum*)	ND	ND	22.01	0.09	12.6	0.7	4.7	0.3	37.2	9368.4	1194.1	0.96	0.13	0.95	0.96	0.13	<5yr	69°14′51″N, 53°32′20″W	0
Vaigat (*Laminaria digitata*)	ND	ND	1.26	0.03	14.1	0.7	5.3	0.3	37.5	474.6	54.7	0.91	0.11	0.92	0.91	0.11	<5yr	70°02′04″N, 52°55′44″W	0
Karratfjord (*Fucus distichus*)	ND	ND	15.29	0.06	14.0	0.7	4.7	0.3	33.6	6459.5	791.9	1.89	0.24	0.99	1.89	0.24	<5yr	71°32′09″N, 53°12′34″W	0
Lithologies																			
KA14 Metagreywacke	ND	ND	0.04	0.000*	85.8	1.6	34.0	0.7	39.7	2.1	0.1	0.44	0.03	0.70	ND	ND	>1 Ga	71°31′30″N, 52°57′53″W	ND
ST24 Gneiss	ND	ND	0.00	0.000*	1.6	0.0*	0.5	0.0*	30.5	17.7	0.8	2.82	0.16	0.69	ND	ND	>2 Ga	70°40′05″N, 51°33′08″W	ND
Basalt	ND	ND	0.17	0.006	19.9	0.3	7.1	0.1	35.8	46.2	2.0	1.31	0.04	0.47	ND	ND	>50 Ma	71°31′01″N, 55°17′29″W	ND
Basalt r	ND	ND	0.17	0.006	18.1	0.3	6.4	0.1	35.6	53.6	2.4	1.36	0.05	0.50	ND	ND	–	–	ND
Core open ocean samples																			
Core SO93 - Laccadive Sea																			
01KL: 0–9 cm	3.19	44.38	16.20	0.05	179.5	0.8	66.1	0.2	36.8	487.5	2.9	1.06	0.01	0.59	1.06	0.01	0.1	07°04′36″N, 79°26′53″E	1688
01KL: 93–100 cm	1.45	46.30	13.87	0.05	130.1	0.6	47.9	0.1	36.8	576.5	3.6	1.06	0.01	0.58	1.06	0.01	9.5	–	
Core SO 189 - Mentawai Strait																			
39KL: 0–6 cm	2.21	19.76	7.79	0.03	215.8	1.3	79.8	0.3	37.0	194.1	1.6	1.02	0.01	0.64	1.02	0.01	0.5	00°47′40″S, 99°54′51″E	571
39KL: 343–348 cm	1.92	18.84	11.72	0.04	142.8	0.7	52.8	0.2	37.0	441.8	3.1	1.02	0.01	0.63	1.02	0.01	10	–	
Core SO 161 - Pacific Ocean																			
22SL: 0–6 cm	2.17	0.52	12.39	0.04	174.5	0.8	64.3	0.2	36.9	383.5	2.3	1.05	0.01	0.57	1.05	0.01	0.5	36°13′16″S, 73°40′50″W	1001
22SL: 250–255 cm	1.54	1.97	16.36	0.05	111.6	0.5	41.2	0.1	36.9	790.6	4.5	1.04	0.01	0.58	1.04	0.01	9.9	–	
Open Gulf of Mexico seaweed																			
Station 5 (*Sargassum fluitans & natans*)	ND	ND	0.27	0.03	67.9	0.9	25.0	0.6	36.8	21.1	2.3	1.06	0.03	0.19	1.06	0.03	<5yr	26°00′07″N, 91°28′04″W	ND
Station 8 (*Sargassum natans*)	ND	ND	0.16	0.03	78.5	0.9	28.9	0.7	36.8	10.9	2.1	1.05	0.03	0.10	1.05	0.03	<5yr	26°00′25″N, 91°04′05″W	ND
Station 30 (*Sargassum natans*)	ND	ND	0.08	0.05	61.2	1.4	22.6	1.1	36.9	6.8	4.6	1.03	0.06	0.07	1.03	0.06	<5yr	26°00′01″N, 88°08′13″W	ND

r indicates repeat analysis.
ND Not determined.
*Indicates uncertainty is less than significant figures stated.
[a] Rho is the associated error correlation function (Ludwig, 1980).
[b] Osi values have been calculated at the deposition age of the sediment e.g., 8.7 ka cal. BP.

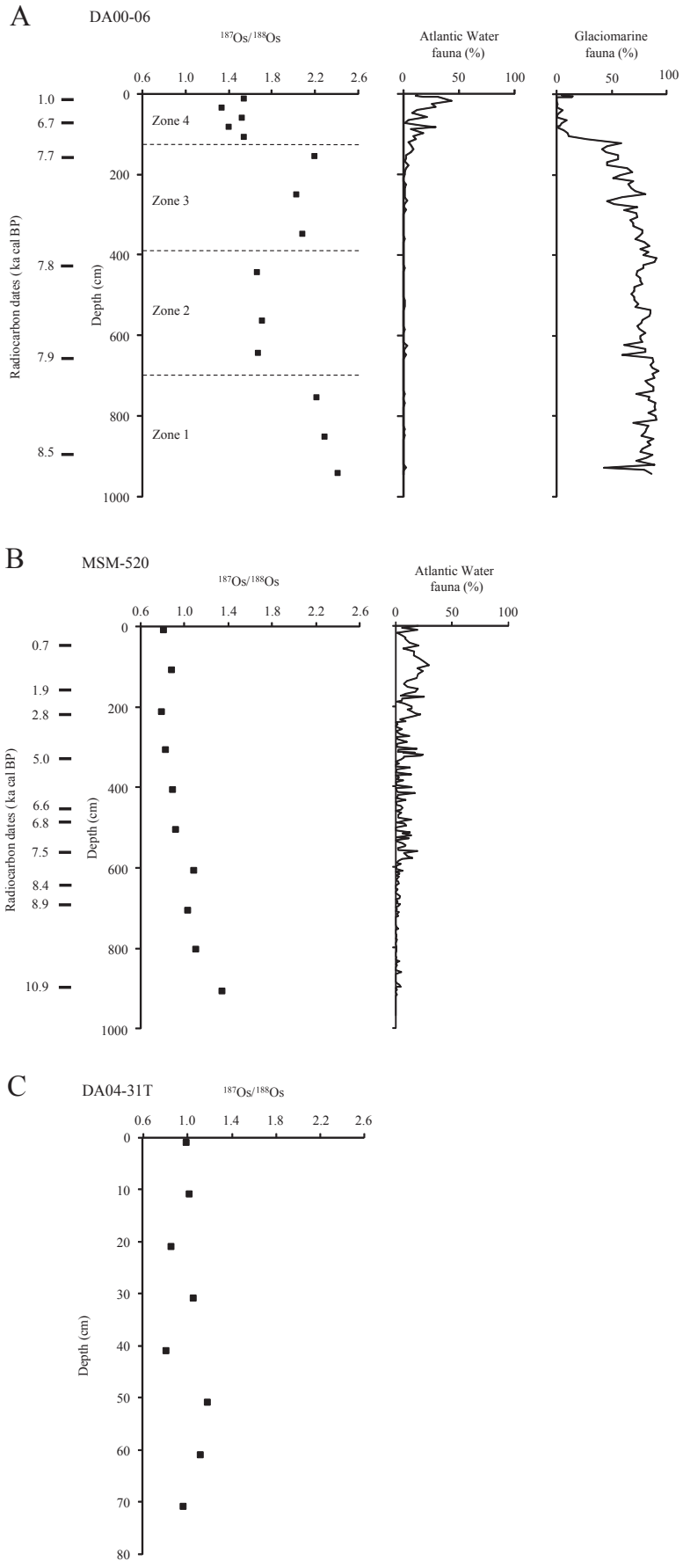
A
DA00-06
$^{187}Os/^{188}Os$
Atlantic Water fauna (%)
Glaciomarine fauna (%)
0.6 1.0 1.4 1.8 2.2 2.6
0 50 100
0 50 100
Radiocarbon dates (ka cal BP)
1.0
6.7
7.7
7.8
7.9
8.5
Depth (cm)
0 200 400 600 800 1000
Zone 4
Zone 3
Zone 2
Zone 1
B
MSM-520
$^{187}Os/^{188}Os$
Atlantic Water fauna (%)
0.6 1.0 1.4 1.8 2.2 2.6
0 50 100
Radiocarbon dates (ka cal BP)
0.7
1.9
2.8
5.0
6.6
6.8
7.5
8.4
8.9
10.9
Depth (cm)
0 200 400 600 800 1000
C
DA04-31T
$^{187}Os/^{188}Os$
0.6 1.0 1.4 1.8 2.2 2.6
Depth (cm)
0 10 20 30 40 50 60 70 80

Table 3
Radiocarbon dates from analyzed cores.

Core	Depth (cm)	Lab code	Material	14C age (yr BP)	Mean calibrated age (yr BP)	Age range 2σ (yr BP)
MSM-520	41	Poz-22364	Shell	1205 ± 30	744	831–666
	161	Poz-22365	Shell	2260 ± 30	1867	1963–1780
	216–218	LuS 8601	Benthic foraminifera	3055 ± 60	2836	2980–2714
	328–330	LuS 8550	Benthic foraminifera	4730 ± 70	4995	5220–4821
	452–456	LuS 8549	Benthic foraminifera	6125 ± 65	6555	6713–6400
	480	AAR-11700	Bivalve	6326 ± 43	6790	6906–6668
	556–560	LuS 8548	Benthic foraminifera	7065 ± 70	7547	7666–7424
	640–642	Poz-30962	Bivalve	7900 ± 40	8364	8457–8279
	692–694	LuS 8547	Benthic foraminifera	8340 ± 70	8896	9106–8655
	896–906	LuS 7707	Benthic foraminifera	9970 ± 100	10,908	11,158–10,630
DA00-06	5–7	KIA-17925	Benthic foraminifera	1500 ± 90	1047	943–1160
	72–76	B203723	Benthic foraminifera	6300 ± 40	6762	6653–6872
	159	AAR-6837	Shell	7350 ± 68	7791	7663–7937
	426–434	KIA-23024	Benthic foraminifera	7270 ± 45	7713	7640–7816
	646–654	KIA-23025	Benthic foraminifera	7430 ± 70	7889	7734–8018
	891	AAR-6839	Shell	7843 ± 72	8321	8154–8416

Using OxCal v4.1 (Bronk Ramsey, 2009).
^{14}C Age (uncorrected), 100% marine, Marine09curve, Delta R = 0 ± 0.
MSM-520 chronology from McCarthy (2011).
DA00-06 chronology from Lloyd et al. (2005) and Hogan et al. (2011).

the $Cr^{VI}O_3$–H_2SO_4 technique) is a faithful record of hydrogenous Re and Os and not detrital Os from silicate minerals and thus suitable for assessing the Holocene $^{187}Os/^{188}Os$ seawater record.

For all samples between 0.2 and 1.6 g of powder was digested in a carius-tube with a known amount of a ^{185}Re–^{190}Os tracer solution with an acid medium (8 mL of 0.25 g/g $Cr^{VI}O_3$–4 N H_2SO_4 for sediments; 9 mL of 1:2 mix of 11 N HCl: 15.5 N HNO_3 for bedrock and seaweed samples) at 220 °C for 48 h. Osmium was isolated and purified from the acid medium using $CHCl_3$ solvent extraction into HBr, and then micro-distillation. Rhenium was isolated and purified using NaOH–C_3H_6O solvent extraction and anion chromatography. The isolated Re and Os fractions were loaded onto Ni and Pt filaments respectively, for their isotopic composition determination using a ThermoElectron TRITON mass spectrometer. Rhenium and Os isotope compositions were obtained using Faraday collectors and the secondary electron multiplier, respectively. Full analytical procedural blanks for this study are 13.2 ± 0.1 pg for Re; 0.13 ± 0.13 pg for Os with an $^{187}Os/^{188}Os$ of 0.264 ± 0.456 (1SD, n = 2 for $Cr^{VI}O_3$–H_2SO_4), and 1.7 ± 0.04 pg for Re; 0.13 ± 0.08 pg for Os with an $^{187}Os/^{188}Os$ of 0.410 ± 0.509 (1SD, n = 2 for HCl:HNO_3). Calculated uncertainties include those associated with mass spectrometer measurements, blank abundance and composition, reproducibility of standard Re and Os isotope values and spike calibration. In-house standard solutions of Re and Os (DROsS) yield an average $^{185}Re/^{187}Re$ value of 0.59806 ± 0.00144 (1SD, n = 257), and $^{187}Os/^{188}Os$ of 0.10693 ± 0.000041 (1SD, n = 178), respectively, which is identical, within uncertainty to the previously published values (Nowell et al., 2008; Rooney et al., 2010). Based on the reproducibility of an organic-rich sedimentary reference sample, SDO-1, we consider only variations in $^{187}Os/^{188}Os \geq 0.04$ between samples to be related to geological processes (Du Vivier et al., 2014, 2015).

4. Results

4.1. Total organic carbon, and Rhenium and Osmium abundances

All Holocene sediments analyzed in this study are characterized as organic-bearing silty-clay. Total organic carbon (Table 4) values for all samples from the DA-04-31T core are variable, ranging from a low of 0.07 wt% at the base of the core to the highest value at the core top of 0.35 wt%. The average TOC value for all samples from the MSM-520 core is 1.25 ± 0.26 (1SD) wt%, ranging from 0.86 to 1.63 wt%. Values tend to increase up core. For DA00-06 TOC values are very low for the lower section of the core (ranging from 0.02 to 0.16 wt% from 940 to 150 cm). Values then increase to 0.31–0.81 wt % from 110 to 10 cm (Table 4). Two surface sediment spot samples have values of 0.14 (Site 4) and 1.77 (MSM-340) wt% TOC (Table 1). Total organic carbon for open ocean samples have similar to slightly higher abundances (TOC = 1.5 to 3.2 wt%; Table 1).

Rhenium and osmium elemental abundances of all Holocene organic-bearing sedimentary samples of this study range between 0.4 and 25.7 ng/g for Re, and 36.5 and 353.5 pg/g for Os. The crustal lithologies gneiss, metagreywacke, and basalt have abundances of 0.004, 0.035, and 0.2 ng/g Re, and *c.* 6, 1.6 and 19 pg/g Os, respectively. The seaweed samples contain between 1.3 and 22.0 ng/g Re and 12.6–14.1 pg/g Os, respectively.

4.2. Osmium isotope ($^{187}Os/^{188}Os$) compositions

The sampled crustal units of the Disko Bugt area have moderate to highly radiogenic $^{187}Os/^{188}Os$ compositions from 0.44 to 2.82. Similar to these values, surface samples and seaweed of the Disko Bugt area have $^{187}Os/^{188}Os$ compositions that range between 0.48 and 2.62. In contrast to highly variable Os compositions of the surface samples of Disko Bugt area, three surface samples from the Laccadive Sea, Mentawai Strait, and Pacific Ocean have values of 1.06, 1.02 and 1.05, respectively. These values are comparable to seaweed collected from surface waters between 26 and 28°N and 87 and 89°W in the Gulf of Mexico ($^{187}Os/^{188}Os$ compositions from 1.03 to 1.06; Table 1).

Core DA04-31T records relatively constant $^{187}Os/^{188}Os$ compositions (1.02 ± 0.12; 1SD, n = 8) throughout the core (Fig. 3C). Core MSM-520 shows a more constant trend to less radiogenic $^{187}Os/^{188}Os$ compositions, decreasing from 1.35 to 0.81 through the interval *c.* 11 to 0.3 ka cal. BP (Fig. 3B). Core DA00-06 records the

Fig. 3. Profiles of sediment samples and cores. (A) $^{187}Os/^{188}Os$ record of core DA00-06 over past c. 9 ka cal. BP with four stages of ice sheet advance and retreat recorded in the core. Panel on the right displays foraminifera frequencies of glaciomarine and Atlantic water species expressed as a % of total specimens counted (from Lloyd et al., 2005); (B) $^{187}Os/^{188}Os$ record of core MSM-520 over past 11.4 ka cal. BP. Panel on the right displays foraminifera frequencies of Atlantic water species expressed as a percentage of total specimens counted (from McCarthy, 2011); (C) Profile of depth against $^{187}Os/^{188}Os$ for core DA04-31T over the past c. 10 ka cal. BP. Uncertainties on Os isotopes are 2σ and are smaller than all data points. See text for full details.

Table 4
Re and Os elemental and isotopic composition data, calibrated ages and sample location details for core sections.

	wt% TOC	% $CaCO_3$	Re (ng/g)	±	Os (pg/g)	±	^{192}Os (pg/g)	±	^{192}Os%	^{187}Re/^{188}Os	±	^{187}Os/^{188}Os	±	rho[a]	Osi[b]	±	Age cal. Kyr[c]	Lat and long	Water depth (m)	1/Os
Core DA00-06 (proximal to Jakobshavn Isbræ)																				
8–16	0.78	0.65	13.90	0.04	71.6	1.5	24.9	0.5	34.8	1109.0	44.7	1.55	0.09	0.71	1.55	0.05	1.50	69°10′21″N, 51°23′71″W	363	0.0401
32–40	0.81	0.47	25.71	0.08	80.7	1.7	28.8	0.6	35.6	90.0	3.6	1.34	0.08	0.71	1.34	0.05	3.50			0.0348
56–64	0.66	0.85	2.63	0.01	95.6	1.2	33.4	0.3	34.9	156.9	3.2	1.53	0.04	0.70	1.53	0.03	5.60			0.03
80–88	0.56	0.77	13.72	0.04	80.2	1.7	28.4	0.6	35.4	962.0	38.7	1.40	0.08	0.71	1.40	0.05	6.85			0.0352
80-88 r	as above	as above	13.21	0.04	76.6	1.6	27.0	0.5	35.2	974.0	39.1	1.44	0.08	0.70	1.44	0.05	6.85			0.0371
104–112	0.31	1.14	9.33	0.03	79.4	1.7	27.7	0.6	34.8	670.4	27.0	1.54	0.09	0.71	1.54	0.05	7.12			0.0361
152–160	0.16	0.98	2.80	0.01	54.7	1.2	17.8	0.4	32.5	313.7	12.6	2.19	0.12	0.71	2.19	0.08	7.63			0.0563
248–256	0.05	1.17	0.62	0.00	53.4	1.2	17.7	0.4	35.4	69.6	2.8	2.02	0.11	0.71	2.02	0.07	7.71			0.0566
344–352	0.04	1.12	0.46	0.00	65.7	1.5	21.6	0.4	33.0	42.7	1.7	2.08	0.12	0.71	2.08	0.07	7.77			0.0462
344-352 r	as above	as above	0.50	0.00	65.0	1	21.5	0.4	32.9	46.2	1.9	2.06	0.12	0.71	2.06	0.07	7.77			0.0466
440–448	0.05	1.16	0.49	0.00	62.8	1.3	21.6	0.4	34.4	44.9	1.8	1.66	0.09	0.71	1.66	0.06	7.83			0.0463
560–568	0.12	0.47	0.78	0.00	102.7	2.2	35.2	0.7	34.2	43.9	1.8	1.71	0.10	0.70	1.71	0.06	7.96			0.0284
640–648	0.10	0.52	0.86	0.00	65.6	1.4	22.5	0.5	34.3	75.6	3.0	1.68	0.10	0.71	1.68	0.06	8.05			0.0444
752–760	0.02	1.23	0.39	0.00	56.2	1.3	18.2	0.4	32.4	42.6	1.7	2.22	0.13	0.71	2.22	0.08	8.17			0.0549
848–856	0.03	1.21	0.40	0.00	42.3	1.0	13.6	0.3	32.2	58.5	2.4	2.29	0.13	0.71	2.29	0.08	8.28			0.0734
940–944	0.07	1.11	0.47	0.00	46.3	1.1	14.7	0.3	31.8	63.8	2.6	2.41	0.14	0.71	2.41	0.08	9.0			0.0678
MSM-520 (52 m NW of the Nuussuaq Pennisula)																				
4 -14.	1.52	0.34	7.18	0.036	180.2	1.0	68.3	0.3	37.9	209.2	1.9	0.81	0.01	0.57	0.81	0.01	0.33	70°48′57″N 56°50′53″W	546	0.0146
106–112	1.59	0.29	9.64	0.031	174.7	1.0	65.6	0.3	37.6	292.2	2.4	0.88	0.01	0.64	0.88	0.01	1.28			0.0152
210–216	1.63	0.32	12.56	0.041	212.9	1.2	80.8	0.3	38.0	309.2	2.4	0.80	0.01	0.62	0.80	0.01	2.66			0.0124
304–310	1.39	0.45	8.11	0.026	149.8	1.1	56.7	0.3	37.8	284.9	3.3	0.83	0.01	0.63	0.83	0.01	4.38			0.0176
306	1.41	0.38	5.81	0.019	144.1	1.2	55.2	0.7	38.3	209.5	2.9	0.73	0.01	0.69	0.73	0.01				0.0181
404–410	1.33	0.20	10.13	0.033	157.7	0.9	59.2	0.2	37.5	340.7	2.8	0.90	0.01	0.63	0.90	0.01	5.83			0.0169
504–510	1.35	0.40	17.55	0.057	137.4	0.9	51.4	0.2	37.4	679.5	6.3	0.93	0.01	0.64	0.93	0.01	6.98			0.0195
506	1.35	0.37	14.75	0.048	100.9	0.5	37.5	0.2	37.1	783.2	5.2	0.99	0.01	0.62	0.99	0.01				0.0267
604–610	1.16	0.38	9.70	0.031	113.2	0.7	41.5	0.2	36.7	464.9	4.3	1.09	0.01	0.65	1.09	0.01	7.98			0.0241
704–710	1.07	0.62	4.22	0.014	112.4	0.7	41.5	0.2	36.9	202.4	1.8	1.03	0.01	0.65	1.03	0.01	9.00			0.0241
800–806	0.97	0.53	8.24	0.027	86.1	0.6	31.5	0.2	36.6	520.4	5.5	1.11	0.02	0.67	1.11	0.01	10.00			0.0317
803	0.99	0.64	1.24	0.004	66.2	1.3	24.2	1.0	36.6	101.9	4.1	1.10	0.06	0.71	1.10	0.04				0.0413
903	0.86	1.02	1.68	0.005	86.8	1.7	32.2	0.6	37.1	104.1	4.2	1.00	0.06	0.71	1.00	0.03				0.0311
904–910	0.91	0.94	2.94	0.010	85.5	0.7	30.5	0.2	35.6	192.3	2.1	1.35	0.02	0.56	1.35	0.01	11.14			0.0328
Core DA-04-31T (130 m SW of Nuuk)																				
0–2	0.35	11.66	9.58	0.01	52.0	0.3	19.2	0.1	37.0	990.6	8.7	1.01	0.01	0.66	1.01	0.01	0.14	62°33′78″N, 54°0′22″W	2525	0.052
10-12.	0.16	6.61	2.05	0.02	36.7	0.2	13.6	0.1	36.9	300.5	2.6	1.04	0.01	0.66	1.04	0.01	1.55			0.0738
20–22	0.16	11.33	1.31	0.02	54.9	0.3	20.6	0.1	37.6	126.7	1.1	0.88	0.01	0.65	0.88	0.01	2.96			0.0485
30–32	0.19	8.00	11.98	0.02	43.1	0.3	15.8	0.1	36.7	1504.4	14.9	1.07	0.01	0.65	1.07	0.01	4.37			0.0631
40–42	0.20	8.54	3.05	0.02	70.4	0.4	26.6	0.1	37.8	228.4	2.0	0.84	0.01	0.65	0.84	0.01	5.78			0.0376
50–52	0.24	3.03	5.61	0.02	44.5	0.3	16.1	0.1	36.2	691.1	6.0	1.19	0.01	0.66	1.19	0.01	7.19			0.062
60–62	0.20	2.19	1.91	0.02	47.6	0.4	17.4	0.1	36.5	218.7	3.0	1.13	0.02	0.59	1.13	0.01	8.60			0.0576
70–72	0.07	1.32	1.35	0.01	41.4	0.3	15.4	0.1	37.1	174.6	1.5	0.98	0.01	0.66	0.98	0.01	10.01			0.065

r indicates repeat analysis.
[a] Rho is the associated error correlation function (Ludwig, 1980).
[b] Osi values have been calculated at 10 ka. Calculated initials are identical to the modern day values at the 2sf level.
[c] Calibrated ages for MSM-520 from McCarthy (2011), DA00-06 from Lloyd et al. (2005) and DA04-31T based on correlation from Knutz et al. (2011).

most radiogenic Os compositions with a general trend towards less radiogenic values up core ($^{187}Os/^{188}Os$ from 2.41 to 1.34). However, in detail, four zones can be identified based on the Os compositions (Fig. 3A). Zone 1 from *c.* 9.0–8.0 ka cal. BP shows a gradual reduction in $^{187}Os/^{188}Os$ composition from 2.41 to 2.22; Zone 2 from *c.* 8.0–7.78 ka cal. BP shows a sharp reduction in $^{187}Os/^{188}Os$ values ranging from 1.66 to 1.71; Zone 3 from *c.* 7.78–7.50 ka cal. BP shows an increase in $^{187}Os/^{188}Os$ values ranging from 2.02 to 2.19 and; Zone 4 from 7.50 ka cal. BP to present shows an abrupt decline to $^{187}Os/^{188}Os$ values averaging 1.55 (Fig. 3A).

5. Discussion

5.1. Consistent records of Os composition in far field sites

The canonical value of present day oceanic $^{187}Os/^{188}Os$ value of 1.06 (1.04 for the North Atlantic and Central Pacific; 1.06 for the Eastern Pacific and Indian Ocean) was from direct analyses of seawater and scrapings of hydrogenetic Fe–Mn crusts (Peucker-Ehrenbrink and Ravizza, 2012 and references therein; Gannoun and Burton, 2014 and references therein). The $^{187}Os/^{188}Os$ values from our surface sediment samples from three non-glacially influenced ocean sites show similar values (Laccadive Sea, 1.06; Mentawai Strait, 1.02; Pacific Ocean, 1.05; Table 1). From these same sites, samples taken at *c.* 10 ka have identical Os values, within uncertainty, to those at the surface (Fig. 2). This indicates that in far-field sites, seawater Os compositions are stable over kyr timescales and are reliably recorded in surface sediments. We also note that the $^{187}Os/^{188}Os$ composition for three open-ocean floating seaweeds from the Gulf of Mexico (1.05 ± 0.01; Table 1; Fig. 2), are identical, within uncertainty of published values, indicating that seaweed directly records the Os isotope composition of seawater.

5.2. Surface sediments in near-field sites

In comparison to the far field sites, surface sediment samples from four sites within the Disko Bugt – Uummannaq region possess highly variable $^{187}Os/^{188}Os$ compositions (0.48–2.62; Table 1; Fig. 2). Surface samples from MSM-540 (100 km west of Disko Island) and MSM-340 (80 km south-west of Disko Bugt), and seaweed from Qeqertarsuaq and Vaigat possess $^{187}Os/^{188}Os$ values close to open ocean seawater (0.98 ± 0.01; 1.13 ± 0.01, 0.96 ± 0.13; 0.91 ± 0.11, respectively; Table 1). In contrast, surface samples from Site 4, the most proximal location to the Jakoshavn Isbræ, MSM-380 (proximal to Disko Island and Nuussuaq which are comprised solely of Paleocene tholeiitic and picritic lavas), and seaweed from the mid-point of Karrat Fjord (adjacent to Karrat Group metasediments) have markedly different $^{187}Os/^{188}Os$ values (2.62 ± 0.05, 0.50 ± 0.03, 1.89 ± 0.24, respectively; Table 1).

As such, these $^{187}Os/^{188}Os$ data indicate that the Os isotope composition of sediments and seaweed from more proximal coastal areas and more distal ocean areas are strongly controlled by regional variations in the Os flux into the ocean; a conclusion consistent with previous Os isotope studies of glacially-influenced marine strata (Paquay and Ravizza, 2012). Further, the marine residence time of Os, that is, the amount of Os dissolved in seawater divided by the sum of input and output fluxes, in these regions will be considerably shorter than the canonical value of *c.* 10^4 yr.

Site 4 has an $^{187}Os/^{188}Os$ value similar to the sampled Archean gneiss (2.62 vs. 2.82), which is the predominant bedrock source of Os from Jakoshavn Isbræ. In contrast, the surface sample from MSM-380 has an $^{187}Os/^{188}Os$ composition (0.49) that is less radiogenic than determined for our basalt sample (*c.* 1.3), which is from the southwest coast of Svartenhuk. However, picrites from Disko Island typically have $^{187}Os/^{188}Os$ values of *c.* 0.13–0.14, and elevated Re and Os elemental abundances (up to 0.8 and 3.4 ng/g, respectively), which suggest the magma originated from a relatively uncontaminated mantle source (e.g., Schaefer et al., 2000). As such, the present day seawater Os value recorded at MSM-380 may represent Os sourced from the unradiogenic Os-bearing Paleocene ultramafic-mafic units of Disko Island and Nuussuaq, and radiogenic Os from the mainland gneiss. Our basalt Re–Os data is supportive of previous models suggesting that parts of the Paleocene magma system assimilated local Cretaceous sediments during eruptions (Goodrich and Patchett, 1991; Ulff-Møller, 1990; Schaefer et al., 2000), which we further demonstrate here using Os isotopes (Table 1). Lastly, seaweed from Karrat Fjord is significantly more radiogenic than the Karrat Group metagreywacke ($^{187}Os/^{188}Os$ = 1.89 and 0.44, respectively), suggesting a strong flux of Os from the Archean gneiss in the Karrat Fjord.

Variations in the general pattern of $^{187}Os/^{188}Os$ values between core sites reflect site proximity to differing sources of Os. Sediment from core DA00-06 (a proximal location to Jakobshavn Isbræ and in a region Archean gneiss with a modern-day $^{187}Os/^{188}Os$ value of 2.82) is more radiogenic on average than sediments from the MSM-520 core (0.73–1.35) and DA-04-31T core (0.84–1.19). In contrast, values from the far-field core DA04-31T are very similar to background open ocean values ($^{187}Os/^{188}Os$ = 1.06). The moderately radiogenic Os isotope values from core MSM-520 most likely reflect the abundance of relatively unradiogenic bedrock in the catchment area (a $^{187}Os/^{188}Os$ value of 0.44 from the Paleoproterozoic metagreywacke and *c.* 1.3 from the Paleocene basalt).

5.3. Tracking GrIS advance and retreats using seawater Os isotope composition

Trends in Os isotopes at near-ice sites can be compared to their known glacial histories. At the LGM the GrIS extended 300–400 km across the continental shelf in the Disko Bugt – Uummannaq region and was grounded at the shelf edge (Ó Cofaigh et al., 2013; Jennings et al., 2014). Radiocarbon dated sediment cores indicate that the western ice margin retreated asynchronously from the shelf edge in the Uummannaq fjord area compared to Disko Bugt. The ice sheet began retreating from the Uummannaq fjord area *c.* 14.8 ka (Jennings et al., 2014). The retreat can then be traced using cosmogenic radiogenic nuclide dating to Ubekendt Ejland within the main part of Uummannaq fjord by 12.4 ka cal. BP, with rapid disintegration and retreat of the ice margin into the inner fjord by *c.* 11–8.7 ka (Roberts et al., 2013).

The Os isotope record for core MSM-520 records a steady decrease in Os values ($^{187}Os/^{188}Os$ = 1.35–0.81) from 9 to 0 ka. These generally less radiogenic Os values suggest a stronger influence of Os from the surrounding basaltic Paleocene lava flows and Paleoproterozoic metasediments ($^{187}Os/^{188}Os$ values of 1.31 and 0.44, respectively, Table 1) and also from less radiogenic open ocean sources ($^{187}Os/^{188}Os$ values of 1.06). The most radiogenic Os values come from the base of MSM-520 at *c.* 11 ka ($^{187}Os/^{188}Os$ = 1.35, Fig. 3B). This section of the core is dominated by a glaciomarine foraminiferal fauna and is deposited just above sediment interpreted as a subglacial till (McCarthy, 2011). Taken together, these results indicate that seawater in the Uummannaq Fjord system was influenced predominantly by the input of glacially eroded material from a proximal calving margin. The steady decline in $^{187}Os/^{188}Os$ values (1.35–0.81; Fig. 3B) up-core in MSM-520 is interpreted to be a consequence of the rapidly retreating Uummannaq ice stream reducing the influence of radiogenic, continentally-sourced Os reaching this location. This interpretation agrees with sedimentology and foraminiferal biostratigraphy from MSM-520 (McCarthy, 2011) and ice stream reconstructions from cosmogenic radionuclide dating of the surrounding area which clearly show ice retreat

to the inner shelf/coastal fjords by *c.* 11 ka (Roberts et al., 2013; Lane et al., 2014). Furthermore, by *c.* 8 ka the increase in abundance of Atlantic water foraminifera indicates a well-established West Greenland Current implying that water masses in the Uummannaq Fjord system were connected to the open ocean, and that sediment flux from the ice margin had declined considerably (McCarthy, 2011). As such, the steady decrease in Os values through core MSM-520 also suggest a decrease in glacially eroded radiogenic material during the Holocene that we interpret to be related to the retreat of the calving ice margin (Fig. 3B). From *c.* 6 ka foraminifera data suggest that a modern oceanographic circulation pattern had began to dominate in the Disko Bugt – Uummannaq fjord area (Perner et al., 2013). Closely matching this interpretation are the extremely similar $^{187}Os/^{188}Os$ compositions (0.83 ± 0.03) from 4.4 ka cal. BP to the core top. The slightly less radiogenic compositions of these upper core samples is likely related to an increase in the flux of unradiogenic Os from the Paleocene lavas, which dominate the coastline.

In the Disko Bugt region, retreat from the shelf edge started slightly later than at Uummannaq, beginning at 13.8 ka cal. BP (Ó Cofaigh et al., 2013). This ice margin retreated across the shelf to a position just west of the entrance to Disko Bugt by *c.* 12.0 ka, with evidence for a minor advance followed by rapid retreat during the Younger Dryas (Ó Cofaigh et al., 2013). The ice margin then retreated through Disko Bugt reaching the inner bay by 10.2 ka cal. BP followed by marked standstills at 9.3 and 8.2 ka cal. BP. The ice reached the present day ice margin by 7.6–6.5 ka cal. BP (Lloyd et al., 2005; Long et al., 2006; Hogan et al., 2011).

Sediment from core DA00-06 (a proximal location to Jakobshavn Isbræ and in a region dominated by Archean gneiss with a modern-day $^{187}Os/^{188}Os$ value of 2.82; Figs. 1A and 2) is more radiogenic on average than sediments from the MSM-520 core (0.73–1.35) and DA-04-31T core (0.84–1.19). Furthermore, given the proximity of DA00-06 to Jakobshavn Isbræ and this relatively restricted embayment we suggest that the Os residence time in this area of West Greenland is considerably shorter than that of the open-ocean value (10^3 vs. 10^4 yr). As a result of this shortened residence time, the Os isotope profile of core DA00-06 will record changes in Os isotope composition with a delay of *c.* 500–1000 yr. Values from core DA04-31T are very similar to background open-ocean values ($^{187}Os/^{188}Os = 1.06$) suggesting this site was not affected by Holocene variations in ice sheet advance and retreat and that the residence time of Os is similar to the open ocean canonical *c.* 10^4 yr. However, there are trends that can be identified from the two glacial proximal cores reflecting changes in sources and delivery of Os through the Holocene connected to the advance and retreat of the GrIS.

At present, core site DA00-06 is proximal to the calving margin of Jakobshavn Isbræ, a major ice stream draining the GrIS, and the core sediments are strongly influenced by radiogenic meltwater from the ice sheet. The basal section of core DA00-06 (960–120 cm) records a brief (<2000 years) interval of rapid sedimentation (13.8 mm a^{-1}) from Jakobshavn Isbræ when it was grounded at the mouth of Jakobshavn Isfjord (Lloyd et al., 2005). In general, as the $^{187}Os/^{188}Os$ values through this core are relatively high (1.34–2.41), we surmise that this reflects a dominant influence of meltwater carrying glacially eroded rock flour from the highly radiogenic Archean gneiss typical for this region (*c.* 2800 Ma gneiss $^{187}Os/^{188}Os = 2.82$; Table 1). However, upon closer examination of the core, four zones of varying Os isotopes can be identified (Fig. 3A; Table 4). The extremely radiogenic Os values ($^{187}Os/^{188}Os = 2.41, 2.29, 2.22$) of Zone 1 (9.0–8.0 ka cal. BP) reflect the strong influence of sediment-laden meltwater sourced from the proximally grounded Jakobshavn Isbræ. This agrees with the sedimentology and benthic foraminiferal assemblage; glaciomarine fauna (Fig. 3A) such as *E. excavatum f. clavata*, *C. reniforme* and *Stainforthia feylingi* (Lloyd et al., 2005). We hypothesize this highly radiogenic Os signal from Zone 1 is indicative of an Os flux sourced from Archean crustal rocks when the ice stream calving margin stabilised and re-advanced at the mouth of the Isfjord between *c.* 10.3 and 8.2 ka (Long and Roberts, 2003; Long et al., 2006; Young et al., 2013). The markedly lower Os isotope values ($^{187}Os/^{188}Os = 1.68, 1.71, 1.66$) of Zone 2 (8.0–7.78 ka cal. BP) are suggestive of a reduction in the flux of radiogenic rock flour to the core site. We suggest that this results from a reduction in meltwater derived glacial rock flour caused by ice margin retreat after the 8.2 ka re-advance event (Young et al., 2013). However, the foraminiferal fauna do not show any major change; the assemblage is still dominated by proximal glaciomarine species. The decrease in Os could therefore be due to a subtle shift in sediment or meltwater flux that is not registered in the foraminifera fauna (Fig. 3A). The increase in Os isotope values ($^{187}Os/^{188}Os = 2.06, 2.08, 2.02, 2.19$) during Zone 3 (7.78–7.5 ka cal. BP) we suggest represents a return to conditions similar to Zone 1 – a finding also supported by the glaciomarine foraminifera assemblage. This increase in Os isotope values could result from greater sediment flux due to ice stream stabilization at the eastern end of the Isfjord, or a minor re-advance, but cosmogenic exposure ages suggest the ice was *c.* 25–30 km east of its 8.2 ka position by this time (Young et al., 2013). The alternative explanation is either an increase in meltwater or ice rafted debris delivery to the core site, which could correlate with increased surface ablation, run-off and calving due to increased air temperatures during the Holocene Thermal Maximum (Carlson and Winsor, 2012). There is an abrupt drop in $^{187}Os/^{188}Os$ values from 2.19 to 1.54 at the transition from Zone 3 to Zone 4 (Fig. 3A). This final shift occurs at 7.5 ka cal. BP; Os values then remain less radiogenic through to the top of the core (112 cm). This coincides with a significant shift in foraminiferal fauna with relatively warmer Atlantic water fauna (indicating a stronger influence from the West Greenland Current) replacing the glaciomarine fauna (Fig. 3A). This shift is likely to be a response to the retreat of the calving front to a distal location up to 20 km inboard of the present ice margin (i.e. Holocene minimum position; Funder et al., 2011; Hogan et al., 2011; Young et al., 2013).

In summary, the pronounced decline in Os isotope values in core DA00-06 resulted from decreasing volumes of meltwater and glacially eroded rock flour as the calving margin of the Jakobshavn Isbræ retreated from the mouth of Jakobshavn Isfjord to its present day location *c.* 50 km further from the core site during the Holocene. The trends in the Os data demonstrate a nuanced pattern of ice margin retreat, re-advance and standstill, broadly correlative with recent onshore deglacial histories (Long et al., 2006; Young et al., 2013). However, those trends contrast somewhat with offshore sedimentological and biostratigraphic evidence, which may not capture subtle shifts in sediment and meltwater flux (Lloyd et al., 2005).

Core DA04-31T located *c.* 200 km southwest of Nuuk beyond the continental shelf (2525 m water depth) records open ocean sedimentation for the entire Holocene epoch (Knutz et al., 2011). Samples throughout the core have broadly similar $^{187}Os/^{188}Os$ values (1.02 ± 0.12) with no discernable trend, indicating a minimal influence from the GrIS in contrast to cores MSM-520 and DA00-06. The DA04-31T core Os values are similar to values for other global sites and present day seawater, especially that of the North Atlantic (Paquay and Ravizza, 2012 and references therein; Gannoun and Burton, 2014 and references therein; Figs. 2 and 3C). The small deviations (≤4%) from the canonical seawater $^{187}Os/^{188}Os$ value of 1.06 may relate to site-specific differences in oceanographic currents and relevant sources of Os (Paquay and Ravizza, 2012).

The data presented here cover a geographical transect from

proximal to distal glacial setting and also temporally from proximal to distal glaciomarine conditions linked to the retreat of major ice streams. We show that Os isotopic signatures can differentiate between proximal glaciomarine settings and more distal open ocean settings. We also show that the isotopic signature can identify shifts in the flux of radiogenic glacially-eroded material and can be used to interpret the relative advance and retreat of marine terminating ice stream margins.

5.4. Implications for seawater heterogeneity and ephemeral Os isotope compositions

Previous Os isotope studies tried to provide records of variations in the intensity of continental weathering on millennial timescales (Sharma et al., 1997; Levasseur et al., 1998; Woodhouse et al., 1999). Integral to these studies is an accurate understanding of the marine residence time of Os. Constraining the residence time of Os in the oceans is challenging, primarily due to its extremely low abundance (*c.* 10 pg/kg; Gannoun and Burton, 2014) although it is thought to be an order of magnitude longer than the mixing time of the oceans, yet significantly shorter than Sr (*c.* 10^4 vs. 10^6 yr; cf. Oxburgh, 1998; Levasseur et al., 1999). The shorter residence time estimates are supported by documented heterogeneities in the modern-day Os seawater composition (Peucker-Ehrenbrink and Ravizza, 2000; Chen and Sharma, 2009; Gannoun and Burton, 2014). The diverse Os values of this study further demonstrate that seawater Os isotope composition is strongly controlled by the oceanographic setting (Paquay and Ravizza, 2012; Du Vivier et al., 2014, 2015).

A lack of absolute constraints for the fluxes of Os from the mainland, Disko island, the volume (and seasonal volume changes) of water, salinity changes (thus likely changes in seasonal behaviour of Os), and sedimentation rates within Disko Bugt hinder attempts to generate a complete model of Os isotope variations for this region. However, the Os isotope data presented in Fig. 4 indicates that Os variations seen in the west Greenland samples can be partially explained as the result of physical mixing between different proportions of isotopically distinct lithogenic material. However, this can only explain mixing in the water column and cannot account for the biological uptake of Os (and Re) in macro-algae (Fig. 4; Table 2). Surface sediment samples proximal to the west Greenland margin form a well defined physical mixing trend that is bounded by bedrock samples, especially if the high concentration and low $^{187}Os/^{188}Os$ picritic basalts reported by Schaefer et al. (2000) are included with the three bedrock lithologies investigated here (not shown on Fig. 4; Table 2).

Core DA00-06 shows significant, rapid changes (*c.* 10^3 yr) in the Os composition of seawater. Previous estimates of the residence time of Os in seawater are significantly greater (e.g., ≥50 kyr; Oxburgh, 2001; Peucker-Ehrenbrink and Ravizza, 2012 and references therein) than the temporal changes observed here. During the Holocene epoch unradiogenic Os inputs directly from magmatic, hydrothermal and extra-terrestrial sources can be considered constant and thus the Os isotope compositions of the studied sites herein are explicitly modulated by silicate weathering of the continental lithologies by the GrIS as discussed above. To explain the rapid changes in Os isotope composition recorded in these samples the Os residence time must be on the order of *c.* 10^3 yr. To shorten the residence time inputs must be changing during deglacial/glacial events, and/or have changing Os isotope composition of the inputs (Oxburgh, 2001).

6. Conclusions

The Os isotope compositions presented here along with palaeoceanographic data demonstrate the ability to identify shifts in the flux of radiogenic glacially eroded material that can be used to track ice sheet advance and retreat patterns. Application of Os isotope stratigraphy in core DA00-06 reveals that the ocean – calving margin interface of the Jakobshavn Isbræ has a more complex history than was previously recorded by the biostratigraphy. Our Os isotope data yields four zones that mark oscillation of the Jakobshavn Isbræ calving margin during the Holocene that broadly correlate with the known deglacial history of the ice stream. These data highlight the potential for Os isotopic signatures to identify shifts in the flux of glacially derived material and ultimately better decode the dynamic behaviour of marine terminating ice streams at millennial timescales.

Our Os isotope values for three seaweeds from the Gulf of Mexico are identical, within uncertainty, of published seawater values, indicating that seaweed directly records the Os isotope composition of seawater. These novel isotope data yield insights into the complexation behaviour of Re and Os into organic matter and provide further context for the application of Re and Os as redox state tracers in ancient sedimentary successions. The Os isotopic profiles from the three cores presented here reveal that seawater Os composition is strongly controlled by the oceanographic setting in terms of the proximity to weathering sources and large-scale oceanic currents. Additionally, this study shows that ephemeral changes (*c.* 10^3 yr) in the Os composition of seawater can

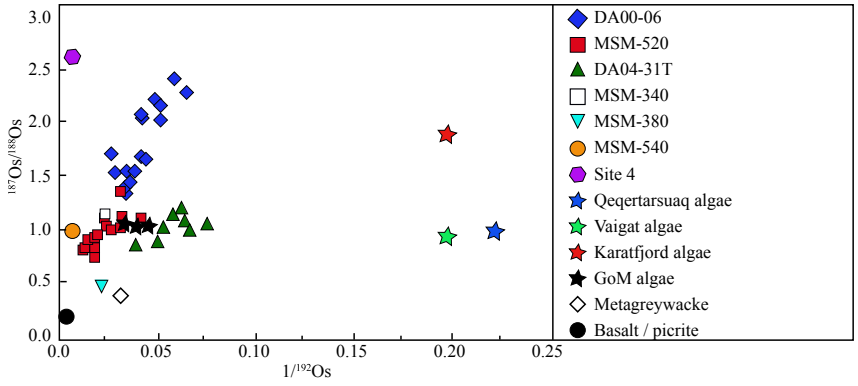

Fig. 4. Simple mixing diagram of Osmium isotope composition of sediment and macro-algae samples plotted against $1/^{192}Os$ to highlight trends in physical mixing of the Disko Bugt region water bodies and related samples. Macro-algae samples do not fit with general mixing trend observed in core samples. Data for basalt/picrite is sample 7712 (their most radiogenic sample) from Schaefer et al. (2000) with ^{192}Os calculated based on a natural abundance of 40.78%. The highly radiogenic Archean gneiss sample ($1/^{192}Os > 2$) is not plotted. GoM algae-Gulf of Mexico macro-algae. See text for further discussion.

be identified which has implications for our understanding of the residence time of Os in the modern ocean.

Acknowledgements

We thank Barbara Stroem-Baris, Antony Long and Sarah Woodroffe for seaweed samples and Brice Rea and Tim Lane for assistance in collecting bedrock samples. We acknowledge the Bundesministerium fuer Bildung und Forschung (BMBF, Bonn) for funding the SO139 (03G01390A) and SO130 (03G0130A) cruises. This paper benefited from constructive criticisms from Greg Ravizza and Bernhard Peucker-Ehrenbrink and valuable discussions with Francis Macdonald, Sierra Petersen and Alice Doughty. An anonymous reviewer and editor Neil Glasser are also thanked for improving this manuscript. Durham authors also wish to acknowledge: NERC CIAF Grant No: 9063/0409, NERC CIAF Grant No: 9106/0411 and NERC Radiocarbon Facility Grant No: 1559.0411.

References

Blum, J.D., Erel, Y.A., 1995. A silicate weathering mechanism linking increases in marine $^{87}Sr/^{86}Sr$ with global glaciation. Nature 373, 415–418.
Bronk Ramsey, C., 2009. Bayesian analysis of radiocarbon dates. Radiocarbon 51, 337–360.
Burton, K.W., Gannoun, A., Parkinson, I.J., 2010. Climate driven glacial-interglacial variations in the osmium isotope composition of seawater recorded by planktonic foraminifera. Earth Planet. Sci. Lett. 295, 58–68. http://dx.doi.org/10.1016/j.epsl.2010.03.026.
Carlson, A.E., Winsor, K., 2012. Northern hemisphere ice-sheet responses to past climate warming. Nat. Geosci. 5, 607–613. http://dx.doi.org/10.1038/NGEO1528.
Chen, C., Sharma, M., 2009. High precision and high sensitivity measurements of osmium in seawater. Anal. Chem. 81, 5400–5406.
Christoffersen, P., Hambrey, M.J., 2006. Is the Greenland ice sheet in a state of collapse? Geol. Today 22, 98–103. http://dx.doi.org/10.1111/j.1365-2451.2006.00561.x.
Colville, E.J., Carlson, A.E., Beard, B.L., Hatfield, R.G., Stoner, J.S., Reyes, A.V., Ullman, D.J., 2011. Sr-Nd-Pb isotope evidence for ice-sheet presence on southern Greenland during the last interglacial. Science 333, 620–623.
Cumming, V.M., Poulton, S.W., Rooney, A.D., Selby, D., 2013. Anoxia in the terrestrial environment during the Late Mesoproterozoic. Geology 41, 583–586.
Dalai, T.K., Ravizza, G., 2006. Evolution of osmium isotopes and iridium as paleoflux tracers in pelagic carbonates. Geochim. Cosmochim. Acta 70, 3928–3942.
Dalai, T.K., Suzuki, K., Minagawa, M., Nozaki, Y., 2005. Variations in seawater osmium isotope composition since the last glacial maximum: a case study from the Japan Sea. Chem. Geol. 232, 87–98. http://dx.doi.org/10.1016/j.chemgeo.2005.04.012.
Du Vivier, A.D.C., Selby, D., Sageman, B.B., Jarvis, I., Grocke, D.R., Silke, V., 2014. Marine $^{187}Os/^{188}Os$ isotope stratigraphy reveals the interaction of volcanism and ocean circulation during Oceanic anoxic event 2. Earth Planet. Sci. Lett. 389, 23–33.
Du Vivier, A.D.C., Selby, D., Condon, D.J., Takashima, R., Nishi, H., 2015. Pacific $^{187}Os/^{188}Os$ isotope chemistry and U-Pb geochronology: synchroneity of global Os isotope change across OAE 2. Earth Planet. Sci. Lett. 428, 204–216 (in press).
Engleman, E.E., Jackson, L.L., Norton, D.R., Fischer, A.G., 1985. Determination of carbonate carbon in geological materials by coulometric titration. Chem. Geol. 53, 125–128.
Farmer, G.L., Barber, D., Andrews, J., 2003. Provenance of Late Quaternary ice-proximal sediments in the North Atlantic: Nd, Sr and Pb isotopic evidence. Earth Planet. Sci. Lett. 209, 227–243.
Finlay, A.J., Selby, D., Gröcke, D.R., 2010. Tracking the Hirnantian glaciation using Os isotopes. Earth Planet. Sci. Lett. 293, 339–348.
Flowerdew, M.J., Tyrell, S., Peck, V.L., 2013. Inferring sites of subglacial erosion using the Pb isotopic composition of ice-rafted feldspar: examples from the Weddell Sea, Antarctica. Geology 41, 147–150.
Funder, S., Kjellerup, K., Kjær, K.H., Ó Cofaigh, C., 2011. The Greenland ice sheet during the last 300,000 years: a review. In: Ehlers, J., Gibbard, P., Hughes, P.D. (Eds.), Quaternary Glaciations—extent and Chronology: a Closer Look: Developments in Quaternary Science, 15, pp. 699–713. http://dx.doi.org/10.1016/B978-0-444-53447-7.00050-7.
Gannoun, A., Burton, K.W., 2014. High precision osmium elemental and isotope measurements of North Atlantic seawater. J. Anal. At. Spectom 29, 2330–2342.
Garde, A.A., Steenfelt, A., 1999a. Precambrian geology of Nuussuaq and the area north-east of Disko Bugt, West Greenland. In: Kalsbeek, F. (Ed.), Precambrian Geology of the Disko Bugt Region, West Greenland. GEUS, Copenhagen, pp. 6–40.
Garde, A.A., Steenfelt, A., 1999b. Proterozoic tectonic overprinting of Archean gneisses in Nuussuaq, West Greenland. In: Kalsbeek, F. (Ed.), Precambrian Geology of the Disko Bugt Region, West Greenland. GEUS, Copenhagen, pp. 141–154.
Goodrich, C.A., Patchett, P.J., 1991. Nd and Sr isotope chemistry of metallic iron-bearing, sediment contaminated tertiary volcanics from Disko Island, Greenland. Lithos 27, 13–27. http://dx.doi.org/10.1016/0024-4937(91)90017-F.
Gregory, J.M., Huybrechts, P., Raper, S.C., 2004. Climatology: threatened loss of the Greenland ice-sheet. Nature 428, 616.
Harris, N.B., Mnich, C.A., Selby, D., Korn, D., 2013. Minor and trace element and Re–Os chemistry of the Upper Devonian Woodford Shale, Permian Basin, west Texas: insights into metal abundance and basin processes. Chem. Geol. 356, 76–93.
Hogan, K., Dix, J., Lloyd, J., Long, A., Cotterill, C., 2011. Near surface stratigraphy of eastern Disko Bugt, West Greenland: implications for glacimarine sedimentation. J. Quat. Sci. 26, 757–766. http://dx.doi.org/10.1002/jqs.1500.
Holland, D.M., Thomas, R.H., de Young, B., Ribergaard, M.H., Lyberth, B., 2008. Acceleration of Jakobshavn Isbræ triggered by warm subsurface ocean waters. Nat. Geosci. 1, 659–664.
Howat, I.M., Joughin, I.R., Scambos, T.A., 2007. Rapid changes in ice discharge from Greenland outlet glaciers. Science 315, 1559–1561. http://dx.doi.org/10.1126/science.1138478.
Huffman, E.W.D., 1977. Performance of a new automatic carbon dioxide coulometer. Microchem. J. 22, 567–573.
Jennings, A.E., Walton, M.E., O'Cofaigh, C., Kilfeather, A., Andrews, J.T., Ortiz, J.D., De Vernal, A., Dowdeswell, J.A., 2014. Paleoenvironments during younger dryas-early holocene retreat of the Greenland ice sheet from outer Disko trough, central west Greenland. J. Quat. Sci. 29, 27–40.
Jonkers, L., Zahn, R., Thomas, A., Henderson, G., Abouchami, W., François, R., Bickert, T., 2015. Deep circulation changes in the central South Atlantic during the past 145 kyrs reflected in a combined $^{231}Pa/^{230}Th$, neodymium isotope and benthic record. Earth Planet. Sci. Lett. 419, 14–21.
Joughin, I., Abdalati, W., Fahnestock, M.A., 2004. Large fluctuation in speed of Jakobshavn Isbræ, Greenland. Nature 432, 608–610. http://dx.doi.org/10.1038/nature03130.
Kendall, B.S., Creaser, R.A., Ross, G.M., Selby, D., 2004. Constraints on the timing of Marinoan 'Snowball Earth' glaciation by $^{187}Re/^{187}Os$ dating of a neoproterozoic post-glacial black shale in Western Canada. Earth Planet. Sci. Lett. 222, 729–740. http://dx.doi.org/10.1016/j.epsl.2004.04.004.
Kendall, B.S., van Acken, D., Creaser, R.A., 2013. Depositional age of the early paleoproterozoic Klipputs Member, Nelani Formation (Ghaap group, Transvaal Supergroup, South Africa) and implication for low-level Re-Os geochronology and paleoproterozoic global correlations. Precambrian Res. 237, 1–12.
Khan, S.A., Aschwanden, A., Bjørk, A.A., Wahr, J., Kjeldsen, K.K., Kjær, K.H., 2015. Greenland ice sheet mass balance: a review. Rep. Prog. Phys. 78 (4), 046801.
Knutz, P.C., Sicre, M.-A., Ebbesen, H., Christiansen, S., Kuijpers, A., 2011. Multiple-stage deglacial retreat of the southern Greenland ice sheet linked with Irminger Current warm water transport. Paleaoceanography 26. http://dx.doi.org/10.1029/2010PA002053. PA3204.
Lane, T.P., Roberts, D.H., Rea, B.R., Rodés, A., Ó Cofaigh, C., Vieli, A., 2014. Ice stream dynamics in the northern sector of the Uummannaq Ice Stream System, West Greenland. Quat. Sci. Rev. 231, 301–313.
Levasseur, S., Birck, J.-L., Allégre, C.J., 1998. Direct measurement of femtomoles of osmium and the $^{187}Os/^{188}Os$ ratio in seawater. Science 282, 272–274. http://dx.doi.org/10.1126/science.282.5387.272.
Levasseur, S., Birck, J.-L., Allégre, C.J., 1999. The osmium riverine flux and the oceanic mass balance of osmium. Earth Planet. Sci. Lett. 174, 7–23. http://dx.doi.org/10.1016/S0012-821X(99)00259-9.
Lloyd, J.M., Park, L.A., Kuijpers, A., Moros, M., 2005. Early Holocene palaeoceanograohy and deglacial chronology of Disko Bugt, West Greenland. Quat. Sci. Rev. 24, 1741–1755. http://dx.doi.org/10.1016/j.quascirev.2004.07.024.
Long, A.J., Roberts, D.H., 2003. Late Weichselian deglacial history of Disko Bugt, West Greenland, and the dynamics of Jakobshavns Isbrase ice stream. Boreas 32, 208–226.
Long, A.J., Roberts, D.H., Dawson, S., 2006. Early Holocene history of the west Greenland ice sheet and the GH-8.2 event. Quat. Sci. Rev. 25, 904–922.
Ludwig, K.R., 1980. Calculation of uncertainties of U–Pb isotope data. Earth Planet. Sci. Lett. 46, 212–220.
McCarthy, D.J., 2011. Late Quaternary Ice-ocean Interactions in Central West Greenland (PhD thesis). Durham University, p. 309.
McManus, J.F., Francois, R., Gherardi, J.M., Keigwin, L.D., Brown-Leger, S., 2004. Collapse and rapid resumption of Atlantic meridional circulation linked to deglacial climate changes. Nature 428, 834–837.
Nick, F.M., Vieli, A., Howat, I.M., Joughin, I., 2009. Large-scale changes in Greenland outlet glacier dynamics triggered at the terminus. Nat. Geosci. 2, 110–114. http://dx.doi.org/10.1038/ngeo394.
Nowell, G.M., Luguet, A., Pearson, D.G., Horstwood, M.S.A., 2008. Precise and accurate 186Os/188Os and 187Os/188Os measurements by multi-collector plasma ionisation mass spectrometry (MC-ICP-MS) part I: solution analyses. Chem. Geol. 248, 363–393.
Ó Cofaigh, C., Dowdeswell, J.A., Jennings, A.E., Hogan, K.A., Kilfeather, A.A., Hiemstra, J.F., Noormets, R., Evans, J., McCarthy, D.J., Andrews, J.T., Lloyd, J.M., Moros, M., 2013. An extensive and dynamic ice sheet on the West Greenland shelf during the last glacial cycle. Geology 41, 219–222. http://dx.doi.org/10.1130/G33759.1.
Oxburgh, R., 1998. Variations in the osmium isotope composition of sea water of the past 200, 000 years. Earth Planet. Sci. Lett. 159, 183–191. http://dx.doi.org/10.1016/j.epsl.2007.08.033.
Oxburgh, R., 2001. Residence time of osmium in the oceans. Geochem. Geophys.

Geosys. 2 paper number 2000GC000104.
Oxburgh, R., Pierson-Wickman, A.-C., Reisberg, L., Hemming, S., 2007. Climate correlated variations in seawater $^{187}Os/^{188}Os$ over the past 200, 000 yr: evidence from the Cariaco Basin, Venezuela. Earth Planet. Sci. Lett. 263, 246–258. http://dx.doi.org/10.1016/j.epsl.2007.08.033.
Paquay, F.S., Ravizza, G., 2012. Heterogeneous seawater $^{187}Os/^{188}Os$ during the Late Pleistocene glaciations. Earth Planet. Sci. Lett. 349, 126–138. http://dx.doi.org/10.1016/j.epsl.2012.06.051.
Paquay, F.S., Goderis, S., Ravizza, G., Vanhaecke, F., Boyd, M., Surovell, T.A., Holliday, V., Haynes Jr., C.V., Claeys, P., 2009. Absence of geochemical evidence for an impact event at the Bølling-Allerød/Younger dryas transition. Proc. Natl. Acad. Sci. 106, 21505–21510.
Perner, K., Moros, M., Snowball, I., Lloyd, J.M., Kuijpers, A., Richter, T., 2013. Establishment of modern circulation pattern at c. 6000 cal. a BP in Disko Bugt, central West Greenland: opening of the Vaigat Strait. J. Quat. Sci. 28, 480–489.
Peucker-Ehrenbrink, B., Ravizza, G., 2000. The marine osmium isotope record. Terra Nova 12, 205–219. http://dx.doi.org/10.1046/j.1365-3121.2000.00295.x.
Peucker-Ehrenbrink, B., Ravizza, G., 2012. Osmium isotope stratigraphy. In: Gradstein, F.M., Ogg, G., Schmitz, M. (Eds.), The Geological Time Scale 2 Volume Set. Elsevier, Amsterdam, pp. 145–166.
Pfeffer, W.T., Harper, J.T., O'Neel, S., 2008. Kinematic constraints on glacier contributions to 21st-century sea-level rise. Science 321, 1340–1343. http://dx.doi.org/10.1126/science.1159099.
Prouty, N.G., Roark, E.B., Koenig, A.E., Demopoulos, A.W.J., Batista, F.C., Kocar, B.D., Selby, D., McCarthy, M.D., Mienis, F., 2014. Deep-sea coral record of human impact on watershed quality in the Mississippi River Basin. Glob. Biogeochem. Cycles 28, 29–43. http://dx.doi.org/10.1002/2013GB004754.
Raiswell, R., Tranter, M., Benning, L.G., Siegert, M., De'ath, R., Huybrechts, P., Payne, T., 2006. Contributions from glacially derived sediment to the global iron (oxyhydr) oxide cycle: implications for iron delivery to the oceans. Geochim. Cosmochim. Acta 70, 2765–2780.
Ravizza, G., Turekian, K.K., 1989. Application of the ^{187}Re-^{187}Os system to black shale geochronometry. Geochim. Cosmochim. Acta 53, 3257–3262.
Rignot, E., Kanagaratnam, P., 2006. Changes in the velocity structure of the Greenland ice sheet. Science 311, 986–990. http://dx.doi.org/10.1126/science.1121381.
Roberts, D.H., Long, A.J., Davies, B.J., Simpson, M.J.R., Schnabel, C., 2010. Ice stream influence on West Greenland Ice Sheet dynamics during the Last Glacial Maximum. J. Quat. Sci. 25, 854–860.
Roberts, D.H., Rea, B.R., Lane, T.P., Schnabel, C., Rodés, A., 2013. New constraints on Greenland ice sheet dynamics during the LGM: evidence from the Uummannaq ice stream system. J. Geophys. Res. http://dx.doi.org/10.1002/jgrf20032.
Rooney, A.D., Selby, D., Houzay, J.-P., Renne, P.R., 2010. Re-Os geochronology of a mesoproterozoic sedimentary succession, Taoudeni basin Mauritania: implications for basin-wide correlations and Re-Os organic-rich systematics. Earth Planet. Sci. Lett. 289, 486–496. http://dx.doi.org/10.1016/j.epsl.2009.11.039.
Rooney, A.D., Chew, D.M., Selby, D., 2011. Re-Os geochronology of the Neoproterozoic-Cambrian Dalradian Supergroup of Scotland and Ireland: implications for neoproterozoic stratigraphy, glaciations and Re-Os systematics. Precambrian Res 185, 202–214. http://dx.doi.org/10.1016/j.precamres.2011.01.009.
Rooney, A.D., Selby, D., Lewan, M.D., Lillis, P.G., Houzay, J.-P., 2012. Evaluating Re-Os systematics in organic-rich sedimentary rocks in response to petroleum generation using hydrous pyrolysis experiments. Geochim. Cosmochim. Acta 77, 275–291.
Rooney, A.D., Macdonald, F.A., Strauss, J.V., Dudas, F.Ö., Hallmann, C., 2014. Selby, D., weathering the snowball. Proc. Natl. Acad. Sci. 111, 51–56.
Schaefer, B.F., Parkinson, I.J., Hawkesworth, C.J., 2000. Deep mantle plume osmium isotope signature from West Greenland Tertiary picrites. Earth Planet. Sci. Lett. 175, 105–118. http://dx.doi.org/10.1016/S0012-821X(99)00290-3.
Selby, D., Creaser, R.A., 2003. Re-Os geochronology of organic-rich sediments: an evaluation of organic matter analysis methods. Chem. Geol. 200, 225–240. http://dx.doi.org/10.1016/S0009-2541(03)00199-2.
Selby, D., Creaser, R.A., Stein, H.J., Markey, R.J., Hannah, J.L., 2007. Assessment of the ^{187}Re decay constant by cross calibration of Re-Os in molybdenite and U-Pb zircon chronometers in magmatic ore systems. Geochim. Cosmochim. Acta 71, 1999–2019. http://dx.doi.org/10.1016/j.gca.2007.01.008.
Sharma, M., Papanastassiou, D.A., Wasserburg, G.J., 1997. The concentration and isotopic composition of osmium in the oceans. Geochim. Cosmochim. Acta 61, 3287–3299. http://dx.doi.org/10.1016/S0016-7037(97)00210-X.
Sperling, E.A., Rooney, A.D., Hays, L., Sergeev, V.N., Vorob'eva, N.G., Sergeeva, N.D., Selby, D., Johnston, D.T., Knoll, A.H., 2014. Redox heterogeneity of subsurface waters in the Mesoproterozoic ocean. Geobiology 12, 373–386.
Straneo, F., et al., 2013. Challenges to understanding the dynamic response of Greenland's marine terminating glaciers to oceanic and atmospheric forcing. Bull. Am. Meteorol. Soc. 94, 1131–1144.
Ulff-Møller, F., 1990. Formation of native iron in sediment-contaminated magma: I. A case study of the Hanekammen Complex on Disko Island, West Greenland. Geochim. Cosmochim. Acta 54, 57–70. http://dx.doi.org/10.1016/0016-7037(90)90195-Q.
Williams, G.A., Turekian, K.K., 2004. The glacial-interglacial variation of seawater osmium isotopes as recorded in Santa Barbara Basin. Earth Planet. Sci. Lett. 228, 379–389. http://dx.doi.org/10.1016/j.epsl.2004.10.004.
Woodhouse, O.B., Ravizza, G., Kenison Falkner, K., Statham, P.J., Peucker-Ehrenbrink, B., 1999. Osmium in seawater: vertical profiles of concentration and isotopic composition in the eastern Pacific Ocean. Earth Planet. Sci. Lett. 183, 223–233.
Young, N.E., Briner, J.P., Axford, Y., Csatho, B., Babonis, G.S., Rood, D.H., Finkel, C., 2011. Response of a marine-terminating Greenland outlet glacier to abrupt cooling 8200 and 9300 years ago. Geophys. Res. Lett. 38, L24701. http://dx.doi.org/10.1029/2011GL049639.
Young, N.E., Briner, J.P., Rood, D.H., Finkel, R.C., Corbett, L.B., Bierman, P.R., 2013. Age of the Fjord Stade moraines in the Disko Bugt region, western Greenland, and the 9.3 and 8.2 ka cooling events. Quat. Sci. Rev. 60, 76e90. http://dx.doi.org/10.1016/j.quascirev.2012.09.028.